Applied Energy 355 (2024) 122259

Contents lists available at ScienceDirect

Applied Energy

journal homepage: www.elsevier.com/locate/apenergy

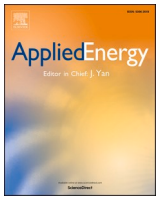

Optimized design and application performance analysis of heat recovery hybrid system for radioisotope thermophotovoltaic based on thermoelectric heat dissipation

Hongyu Wang [a], Zhiheng Xu [a,b,*], Chen Wang [a], Zongbin Hou [a], Mingxin Bian [a], Nailiang Zhuang [a,b], Haijun Tao [c], Yuqiao Wang [d], Xiaobin Tang [a,b,*]

[a] Department of Nuclear Science and Technology, Nanjing University of Aeronautics and Astronautics, Nanjing 211106, China
[b] Key Laboratory of Nuclear Technology Application and Radiation Protection in Astronautics, Ministry of Industry and Information Technology, Nanjing 211106, China
[c] College of Material Science and Technology, Nanjing University of Aeronautics and Astronautics, Nanjing 211100, China
[d] Research Center for Nano Photoelectrochemistry and Devices, School of Chemistry and Chemical Engineering, Southeast University, Nanjing 211189, China

HIGHLIGHTS

- The novel I/W TPV-TE-HRL heat recovery hybrid system was proposed.
- The W-type TPV-TE heat recovery hybrid system with gain of 12.9% at 1000 K.
- The output power of TPV cell and W-type TE-HRL can be increased by 21.6% in series mode.
- W-type TE-TPV series can reach 11.23% energy conversion efficiency when used in deep space.

ARTICLE INFO

Keywords:
Radioisotope thermophotovoltaic generator
Heat recovery
Thermoelectric
Series and parallel connection
Space application

ABSTRACT

Radioisotope thermophotovoltaic (RTPV) generators face a fundamental challenge, which is the significant output loss and energy wastage caused by the substantial thermal deposition resulting from the arrival of infrared radiation from the heat source at the energy conversion unit. This contradiction has gradually become a key limiting factor for its further development in recent years. In this work, a novel hybrid system based on the thermophotovoltaic-thermoelectric (TPV-TE) effect is proposed, in which the Bi_2Te_3-based I/W-type thermoelectric leg plays both heat dissipation and heat recovery for power supply. The heat recovery thermoelectric legs were prepared using a cold pressing mould and sintering method, and their Seebeck effect was used to convert the unwanted heat recover from InGaAs thermophotovoltaic cells into electrical power. The design preparation scheme of the heat recovery hybrid module and its potential application performance at 700–1000 K heat source temperature were investigated through experimental tests and simulations. The W-type TPV-TE heat recovery hybrid system exhibits good gain of 12.9% at 1000 K, and the output power can be increased by additional 21.6% in series mode. Simulations for environmental applications show better heat recovery in deep space than on Earth, with an output gain of 63.7% and an energy conversion efficiency of 11.23%. The heat recovery design enhances the competitiveness of the RTPV and provides new ideas for optimizing other heat recovery applications for thermal energy conversion systems.

1. Introduction

A highly reliable power supply system is an important prerequisite to ensure the smooth conduct of space exploration missions such as deep space and Mars. Nuclear batteries convert the decay energy of radioisotope sources into electrical energy and have the advantages of long-life, high-energy density, continuous self-powering, and independence from environmental influences. They have been extensively used in space exploration missions [1–3]. For example, the Mars Rover Curiosity operating in the Martian atmosphere, the Voyagers and Cassini-Huygens probes in deep space exploration, nuclear batteries have

* Corresponding authors at: Department of Nuclear Science and Technology, Nanjing University of Aeronautics and Astronautics, Nanjing 211106, China.
E-mail addresses: xuzhiheng@nuaa.edu.cn (Z. Xu), tangxiaobin@nuaa.edu.cn (X. Tang).

https://doi.org/10.1016/j.apenergy.2023.122259
Received 3 June 2023; Received in revised form 15 September 2023; Accepted 2 November 2023

Nomenclature

a	thermal diffusivity, m^2/s
c	speed of light, m/s
C	heat capacity at constant volume, J/mol·K
E_b	radiation heat dissipation power density, mW/cm^2
F_v	view factor
FF	fill factor
h	Planck's constant
h_c	convective heat transfer coefficient, $W/m^2 \cdot K$
I	output current, mA
I_{sc}	short-circuit current, mA
I_0	reverse saturation current, mA
k	Boltzmann's constant
$M(\lambda)$	blackbody radiation power density, mW/cm^2
n	idea factor
P_{max}	maximum output power, mW
q	elementary charge, C
$QE(\lambda)$	quantum efficiency
R_L	external load resistance, Ω
R_{in}	internal resistance, Ω
R_c	contact resistance, Ω
T	surface temperature of heat source, K
T_f	temperature of Ambient, K
T_a	temperature of TPV cell, K
V	output voltage of the RTPV, V
V_{oc}	open-circuit voltage of the RTPV, V
ZT	figure of merit of thermoelectric materials
Φ	heat flux, J/m^3
α	seebeck coefficient μV/K
ε	surface emissivity
ρ	density of materials, g/cm^3
κ	thermal conductivity, W/m·K
σ	electrical conductivity, S/m
η	energy conversion efficiency
λ	wavelength, nm
Δ	Laplace arithmetic

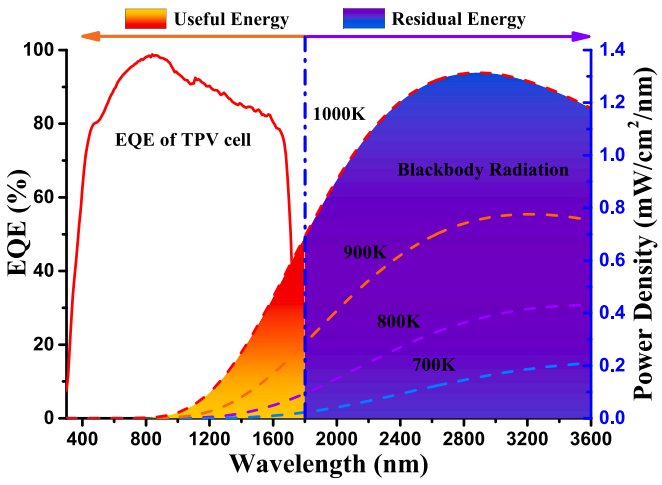

Fig. 1. Mismatch between blackbody infrared radiation and the quantum corresponding interval of the TPV cell.

played a key role in all of these missions [4]. In recent years, more efficient novel radioisotope thermophotovoltaic (RTPV) generators have drawn extensive attention [5–7]. The high quality form of radioisotope energy, near infrared light, is used as a medium for energy transfer and conversion, providing higher energy conversion efficiency and power density [8]. Therefore, the RTPV generators are promising new generation of nuclear power systems for space applications [9].

The infrared radiation in RTPV carries a high energy density, and the attendant problem is the inevitable large amount of thermal deposition in thermophotovoltaic (TPV) cells. Furthermore, there was a serious mismatch between the infrared radiation represented by the blackbody radiation and the corresponding interval of the TPV cell [10], as shown in Fig. 1. Most of the infrared light cannot be converted into electricity by the TPV cell and is deposited as heat, and the temperature of the TPV cell increases even further. Nevertheless, the performance of TPV cell is significantly affected by temperature [11–13]. In previous study, the output power of TPV cell was even reduced to 50% at 340 K compared to 300 K [14]. Therefore, a large amount of excess heat deposition will lead to serious energy and power loss, and the residual heat problem is the most important factor hindering the improvement of the energy conversion efficiency of RTPVs, and it is imperative that the heat recovery and utilization of TPV cells be optimized.

In order to avoid the effects of high temperatures caused by residual heat, powerful active cooling system was often employed to cool down the cell and ensure its efficient and stable energy conversion. However, the active cooling requires additional energy to maintain, which offsets the advantages of the RTPV as a standalone power supply [15]. Current researchers on TPV systems have focused on the modulation of infrared radiation to have the effect of reducing residual heat and improving energy efficiency. The selective emitters and filters have been applied to effectively modulate the infrared spectrum emitted by the heat source to keep the spectral range within the response interval of the TPV cell. For example, Wang et al. [16] and Sakakibara et al. [17] used the photonic confinement properties of photonic crystals to modulate the infrared emission from a heat source. Wang et al. [18] designed an HfO_2/Mo/HfO_2 TPV absorber-emitter that achieves an excellent selective emission cutoff at 1.8 μm. Li et al. [19] used Si/SiO_2 filters to adequately filter and modulate the infrared spectrum. In our previous studies, the proposed core-shell nanosphere photonic crystal emitter achieves an emissivity of >0.93 for $\lambda < 1.72$ μm and < 0.13 for $\lambda > 1.90$ μm [20]. The spinel ferrite coating has a high emissivity of >0.93 and excellent high temperature and irradiation stability [21]. All of the above-mentioned works have significantly improved the infrared radiation efficiency inside the RTPV system. With the above scheme, the infrared radiation efficiency inside the RTPV system is significantly improved. In addition, optical filters and reflective cavity mirrors have been proposed to improve the surface irradiation uniformity of the TPV cell by 87.5% and to reduce its surface temperature by 9–14 K, which fully optimize the transmission and uniformity of infrared radiation inside the RTPV [10,22]. In summary, most of the current studies have been conducted to optimize the absorption response efficiency of TPV cells by modulating the thermal radiation spectrum, whereas little attention has been paid to the heat dissipation and waste heat utilization of the TPV cell. However, if the TPV cell is inherently hot, it is still difficult to utilize infrared radiation efficiently even though the spectrum has been fully optimized, due to the fact that high temperatures can lead to performance degradation.

It is an effective solution to further recover the heat from the TPV cell and convert it into electricity, and then reduce its temperature. In the field of heat recovery, the use of thermoelectric (TE) modules for the recovery of industrial waste heat from chimneys and automobile engines has great potential for application [23,24]. For example, Luo et al. [25] conducted a fluid-thermal-electric multiphysics numerical approach to the waste heat of automobile exhaust using the TE module. Ge et al. [26]

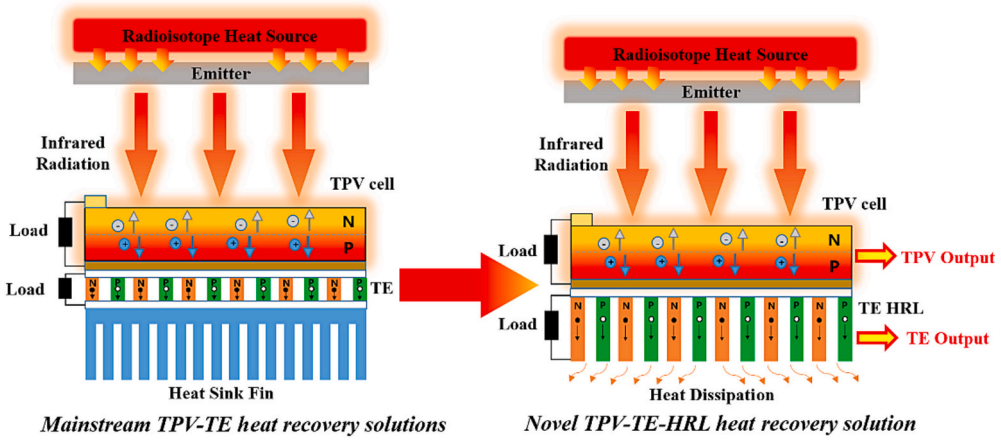

Fig. 2. The proposed novel TPV-TE-HRL heat recovery solution based on the Mainstream TPV-TE solution.

also used a genetic algorithm to geometrically optimize the segmented thermoelectric generator (STEG) module of a waste heat recovery system. However, the application scenarios for heat recovery mentioned above, and even factors such as volume, size, and form of heat source, are so different from RTPV systems that it is difficult to provide an effective reference.

In the field of solar cells, which face the same problem of PV cell heat recovery, the mainstream solutions is the also use of TE modules to reuse the heat deposited in the solar cell and convert it into electricity to improve the overall energy efficiency [27–29]. Shittu et al. [30–32] have carried out a comprehensive study of photovoltaic-thermoelectric (PV-TE) system in recent years using both modeling and experimental approaches. The influence of contact thermal resistance and heat transfer design of PV-TE systems in coupled structures under various conditions was fully discussed. In the concentrating photovoltaic (CPV) system, heat is accumulated rapidly on the PV cell due to the large focusing of sunlight. Therefore, there are a lot of researches on heat recovery and utilization by TE in CPV. For example, Yin, Kil and Lamba et al. [15,33,34] designed a CPV-TE hybrid system with Fresnel optical concentrator, which better improves the output efficiency of the system. In addition, spectral splitting of sunlight using a dichroic mirror for energy conversion using PV and TE respectively is also a novel scheme. Alnajideen et al. [35] constructed a novel hybrid PV-TE system using four dichroic mirrors arranged in a crossed V-trough configuration to split the solar spectrum and then convert the energy, which demonstrate the feasibility of improving the overall efficiency of light-to-electricity conversion based on spectral splitting strategy. Other feasible solutions have also been explored, such as Kim et al. [36] by adding an exothermic reactive interlayer between the PV and TE to enhance the output power of the system. Zhang et al. [37] spliced two PV cells in the PV-TE system into a V-type groove at right angles in order to enhance the absorption of sunlight, and removed the ceramic plate of the TE system to reduce the thermal resistance.

Nevertheless, in the PV-TE hybrid system discussed above, the heat transfer capability of the thermoelectric module is poor. This has a slight effect on solar cells, but when it is applied to an RTPV system with a thermal density many times greater, the heat received by the TPV cell is difficult to carry away quickly. This creates a large amount of heat build-up on the back of the TPV cell, which severely hampers the output efficiency of the TPV cell and have the opposite effect of further power loss. Furthermore, the heat dissipation conditions in the space and Mars environments are very different from those on Earth, so that the traditional heat sink fin design becomes unsuitable. It is necessary to redesign the heat recovery structure of the RTPV for the specific application requirements.

Therefore, in order to solve the problem of energy loss of RTPV caused by thermal deposition and waste heat, this study proposes a "waste-to-energy + energy reuse" approach, which integrates heat dissipation and waste heat to electricity output. In this work, in order to ensure the TPV cell at the suitable temperature and also to recovery the excess heat energy to further improve the energy conversion efficiency, a novel heat recovery hybrid system based on TE fin heat dissipation was proposed, as shown in Fig. 2. The TE module was designed as a heat sink for the TPV cell and was prepared using a cold press mould and sintering

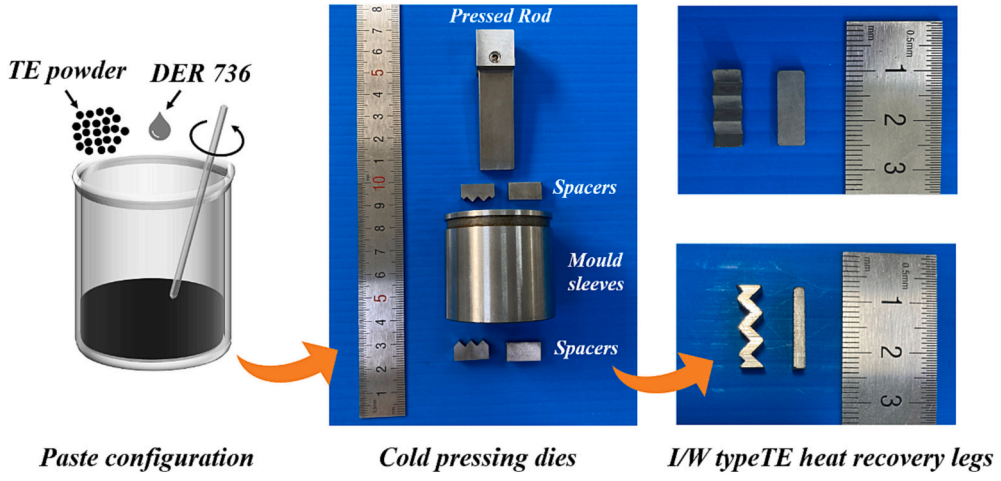

Fig. 3. Preparation process for TE heat recovery legs.

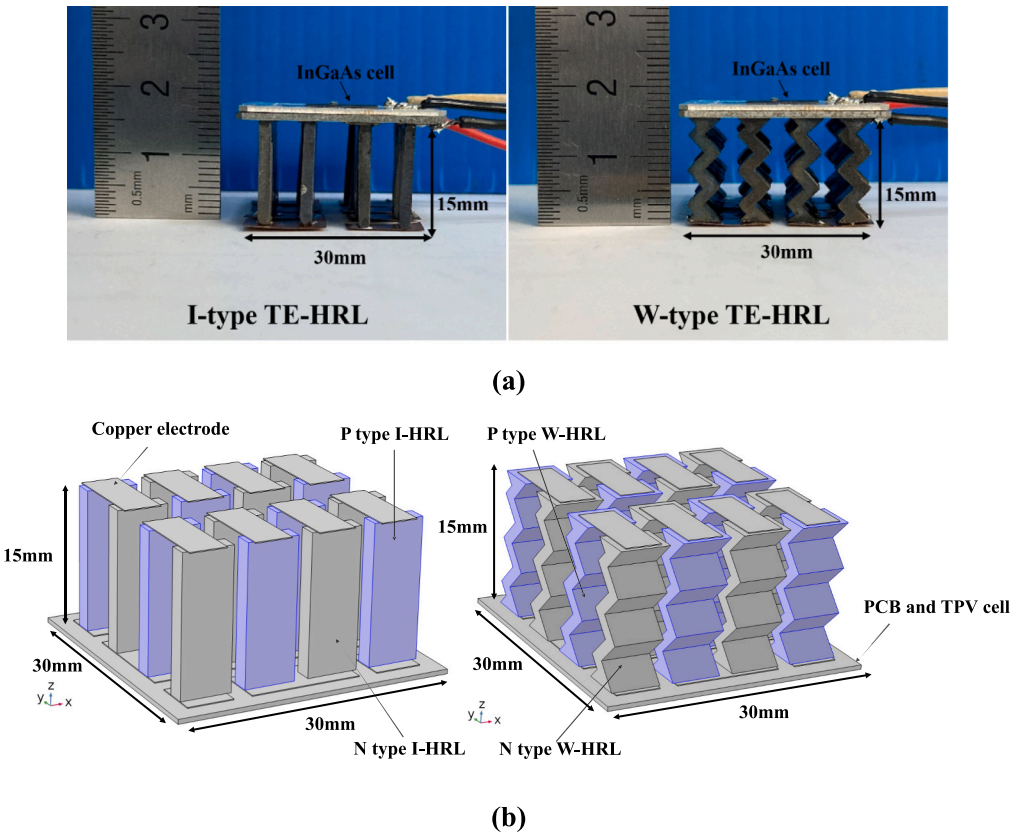

Fig. 4. I-type and W-type TPV–TE HRL heat recovery module (a) photographs, and (b) model drawing.

method. Compared with the mainstream TPV-TE solution, the design in this paper better optimizes the heat dissipation and heat recovery in RTPV, and also solves the problems of thermal deposition and interfacial heat loss encountered therein. In addition, the circuit optimization and space environment operation characteristics of the system were further investigated. The proposed heat recovery system can further improve the heat utilization efficiency, reduce the power loss and increase the output power of the RTPV. This provides new optimization ideas for the future development of next generation space nuclear power systems.

2. Materials and methods

2.1. Design and preparation of RTPV-TE heat recovery modules

2.1.1. Preparation of TE heat recovery legs

The TE heat recovery legs (TE-HRL) with diverse structures were manufactured by cold–press moulding and sintering method [38,39]. This method allows complex 3D thermoelectric parts with excellent electrical properties to be easily prepared from moulds. The preparation process is shown in Fig. 3. First, the P/N Bi_2Te_3-based powders doped with Sb or Se were mixed with DER736 binder (Polyethylene glycol diglycidyl ether) at a mass ratio of 10:1, a stable thermoelectric slurry was obtained after thorough shaking and stirring. In this case, the selection of the ratio of DER736 to TE powder was optimized from previous studies [39]. Next, the thermoelectric slurry was filled into a cold press mould and pressed into shape at a pressure of 2 MPa and ambient temperature for 20 min. This operation can effectively improve the thermal conductivity, electrical conductivity, and structural steel properties of TE-HRL. Finally, the obtained preliminary samples after careful demoulding were sintered at 573.15 K for 4 h under N_2 gas protection, several TE-HRLs of P/N-type were prepared. DER736 contains a variety of binders and diluents that can effectively bind and crystallise the molecular linkages in TE-HRL during high temperature sintering to improve electrical properties.

Two types of TE-HRL were prepared by changing the spacer of the cold press mould. The I-type TE-HRL has a size of 15*5.5*2 mm^3 and was bent on the basis of I-type to obtain W-type TE-HRL, as shown in Fig. 3. To ensure consistency in thickness, the quality of the filled thermoelectric slurry was carefully controlled during preparation. The lead-free solder paste ($Sn_{96.5}Ag_{3.0}Cu_{0.5}$) was evenly applied to the top and bottom of the P/N TE-HRLs, which were placed sequentially on a customized aluminum printed circuit board (PCB) substrate in a π-shaped connection, with their tops connected in series using copper electrode plates. The bonded HRL devices were heated to 410 K and the solder paste was melted sufficiently to fill the connection between the TE-HRL and the electrode, and then rapidly reducted to room temperature and was firmly soldered.

2.1.2. Parameters of the TPV-TE heat recovery module

The TPV cell has a specific absorption range for infrared radiation and requires series III-V semiconductors with a narrow band gap. The direct bandgap InGaAs cell was very widely used in TPV systems due to its high quantum efficiency in-band. As shown in Fig. 4, the InGaAs (E_g = 0.72 eV) cell was fabricated on the backside of the PCB carrying the TE-HRL. The InGaAs cell can form a good thermal contact with 8 pairs of TE-HRLs and form TPV-TE heat recovery module. Here, in order to further improve the heat dissipation of the module and the temperature difference between the hot and cold ends of the TE HRL, an optimized W-type design was proposed on the basis of the I-type. This work provides a preliminary optimization of the dimensions of TE-HRL, whose optimal dimensions need to be analyzed and discussed according to the actual environmental conditions.

2.2. Simulation calculation method

2.2.1. COMSOL finite element simulation

The W/I-type TPV-TE heat recovery moduel was built by using COMSOL Multiphysics software. The shape, dimensions, and material parameters of the InGaAs cell and P/N TE-HRL were substituted into the model and the free tetrahedral micro-element meshing was carried out according to physical field operations. Using the finite element simulation (FEM) method, the coupling analysis of heat transfer, current and thermoelectric effect was conducted. The simulation model was placed in an open space with no wind, at an ambient temperature of 293.15 K and a pressure of 1 atm. The thermodynamic energy transfer model for the entire TPV-TE heat recovery system is described below:

Infrared radiation is emitted from an incandescent radioisotope heat source with an emitter. Following this, the infrared radiation reaches the TPV cell where the light energy is converted into electrical energy using the photovoltaic effect. The infrared radiation that cannot be converted by the TPV cell is converted into thermal energy, which is conducted through the Al-PCB board to the TE-HRL. It is worth noting that, the Al-PCB board is considered as a fully reflective mirror, the infrared radiation emitted by the heat source does not pass through the PCB and act on the TE-HRL, and its heat is supplied entirely by the contact heat conduction of the TPV cell. During the heat transfer process within the TE-HRL, the temperature difference is generated at its two ends. By the Seebeck effect, thermal energy is converted into electrical energy. The remaining heat is then dissipated to the environment through the TE-HRL.

For comparative analysis, the TPV models with heat sink fins (HSF) and with TE-HSF were also constructed and simulated. The heat transport process of the TPV-TE heat recovery module conforms to Planck's blackbody radiation law and the three-dimensional steady-state Fourier heat transfer Eq. [40]:

$$M(\lambda,T)=\varepsilon(\lambda)\frac{2hc^2}{\lambda^5\left(e^{\frac{hc}{\lambda kT}}-1\right)} \tag{1}$$

$$\frac{\Phi}{\rho C}=\frac{\partial u(T,x,y,z)}{\partial T}-a\Delta \tag{2}$$

The radiation spectrum at the surface of the radioisotope heat source is M, influenced by the surface emissivity ε and the temperature of the heat source T, while the heat transfer and temperature distribution are mainly related to the received heat flux Φ, material density ρ, heat capacity C, and thermal diffusivity a.

The boundary conditions of the module in the heat transfer process are radiation heat dissipation E_b and convective heat transfer Q_c, which are mainly influenced by the boundary heat dissipation area A, and the thermal convection coefficient h_c. In addition, the difference between the surface temperature T and the ambient temperature T_f is also an important factor.

$$E_b(T)=\varepsilon A\frac{2\pi^5k^4}{15c^2h^3}\left(T^4-{T_f}^4\right) \tag{3}$$

$$Q_c(T)=h_cA\left(T-T_f\right) \tag{4}$$

2.2.2. Calculation of the electrical output of TPV cells and TE-HRL

Based on the irradiance parameters of the TPV cell surface derived from the COMSOL simulations, the relationship between voltage (V) and current (I) of the InGaAs TPV cell can be calculated numerically using the Shockley function [41]:

$$I=I_{sc}-I_0\left(exp\left(\frac{q}{nkT_a}\left(V+IR_s\right)\right)-1\right)-\frac{V+IR_s}{R_{sh}} \tag{5}$$

$$I_{sc}=q\cdot F_v\int_0^{\infty}\frac{\lambda}{hc}M(\lambda)QE(\lambda)d\lambda \tag{6}$$

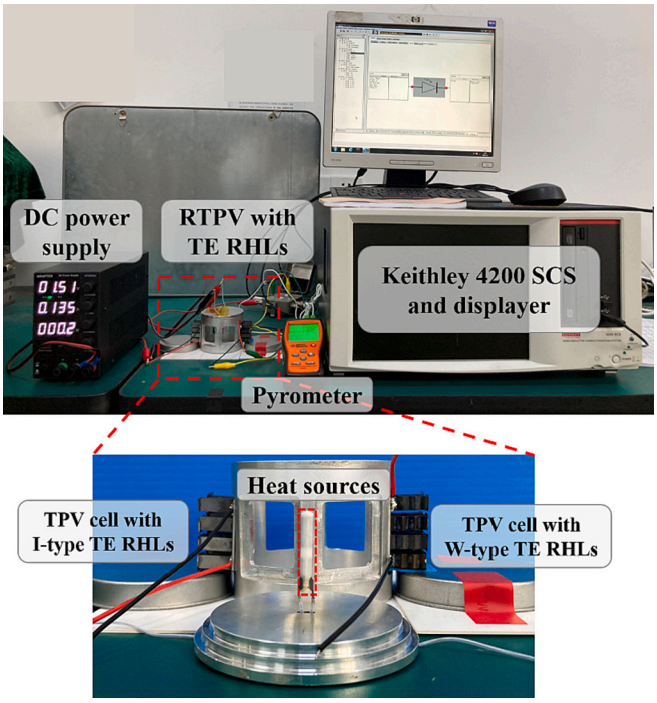

Fig. 5. The test platform for electrical and temperature testing of the InGaAs cells and TE-HRL.

$$P_{TPV}=Max(V\cdot I)=FF(V_{oc}\cdot I_{sc}) \tag{7}$$

The I_{sc} is the short-circuit current, influenced by the radiation spectrum M and the view factor Fv. In addition, the calculated I-V curve depends on the intrinsic parameters of the TPV cell: the external quantum efficiency $QE(\lambda)$, the dark current I_0, the series electrical resistance R_s, the shunt electrical resistance R_{sh}, and the ideality factor n. The above intrinsic parameters can be obtained by testing InGaAs cells in the laboratory. The maximum output power of the TPV cell (P_{TPV}) was selected for comparative analysis, which was calculated from I_{sc}, open circuit voltage V_{oc}, and fill factor FF.

The potential difference V_{oc} of the TE-HRL can be expressed using the Seebeck formula, N being the number of legs, α_p and α_n being the Seebeck coefficients of the P-type and N-type TE-HRLs, respectively. The output power of TE-HRLs is related to their internal resistance R_{in} and the external resistance R_L of the connected device. The maximum output power P_{TE} is obtained when $R_L=R_{in}$. The internal resistance R_{in} consists of the TE-HRL resistance R_{HRL} and the welding resistance R_c. R_{HRL} is related to the current path l, the cross-sectional area S, and the electrical conductivity σ. while R_c is related to the surface coefficient of the weld material K_c, the contact form factor m, and the contact welding pressure F.

$$Voc=N\cdot\left(\alpha_p-\alpha_n\right)\cdot\Delta T \tag{8}$$

$$P_{TE}=\frac{{V_{oc}}^2}{\left(R_{in}+R_L\right)^2}R_L \tag{9}$$

$$P_{\max}=\frac{{V_{oc}}^2}{4R_{in}} \tag{10}$$

$$R_{in}=R_{HRL}+R_c=N\left(\frac{l}{S\sigma}+\frac{2K_c}{F^m}\right) \tag{11}$$

$$\eta=\frac{P_{TPV}+P_{TE}}{Q_{rad}}=\frac{P_{TPV}+P_{TE}}{F_v\int_0^{\infty}M(\lambda,T)d\lambda} \tag{12}$$

The energy conversion efficiency η for the TPV-TE heat recovery

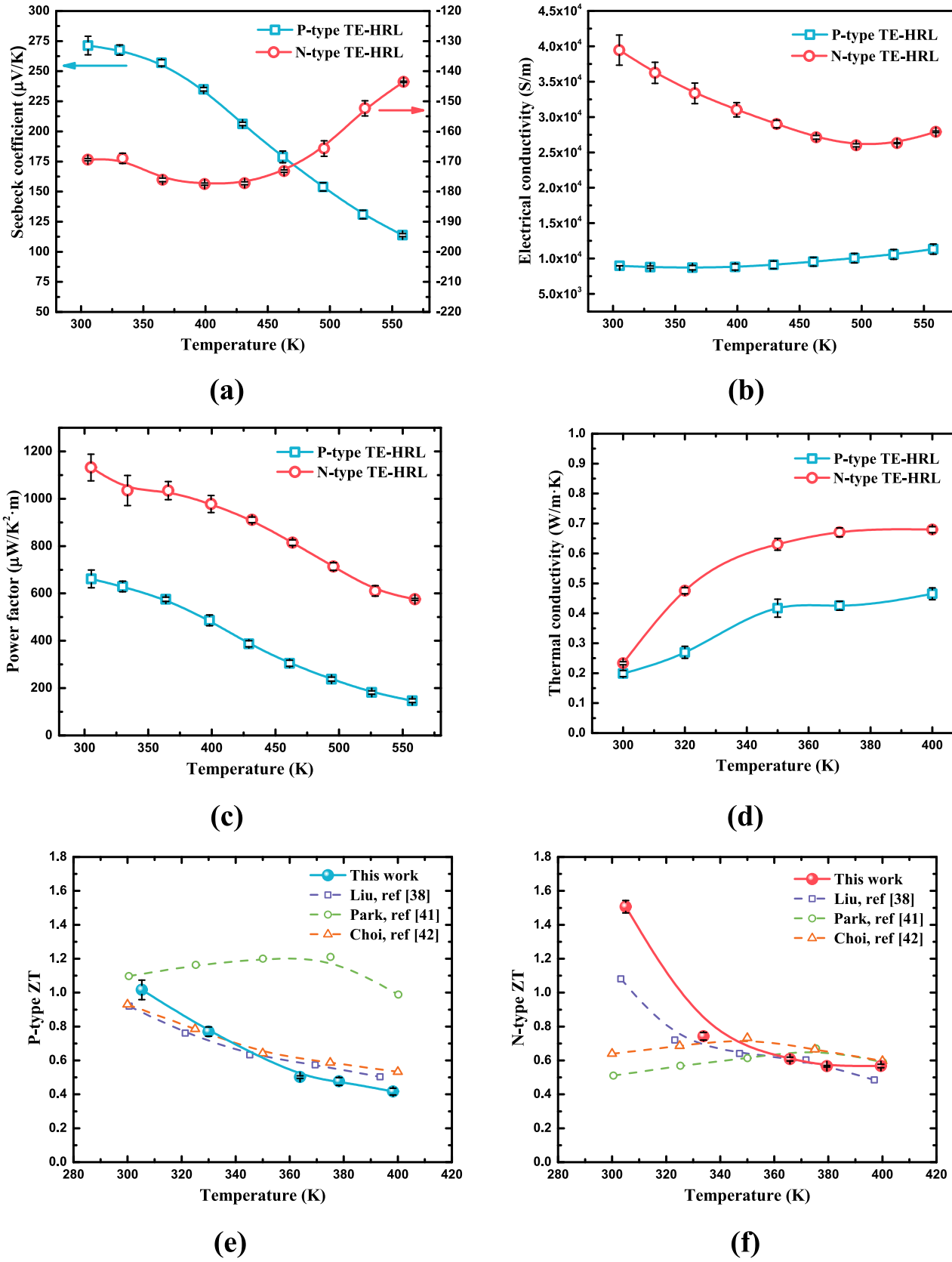

Fig. 6. Thermoelectric properties of the P/N–type thermoelectric materials prepared by the cold–press moulding and sintering method. (a) Seebeck coefficient, (b) electrical conductivity, (c) power factor, (c) electrical conductivity, and ZT of the (e) P–type and (f)N–type in comparison with the previously reported Bi_2Te_3–based paints.

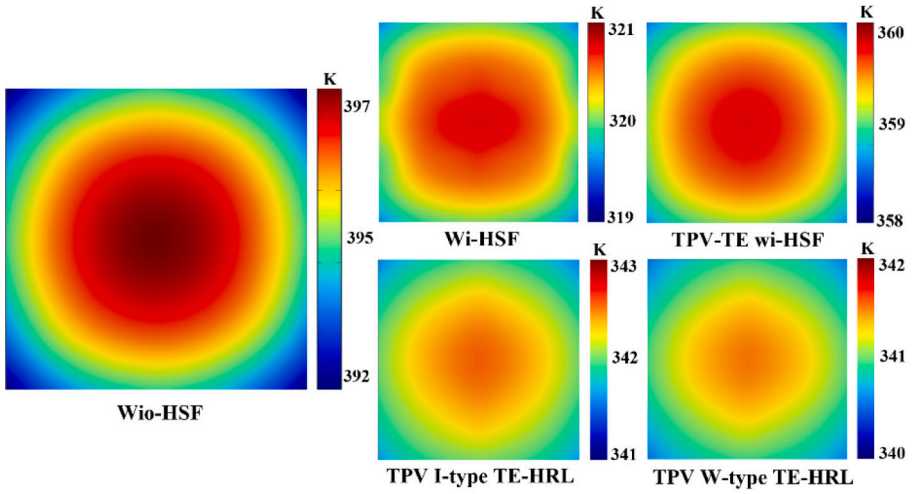

(a)

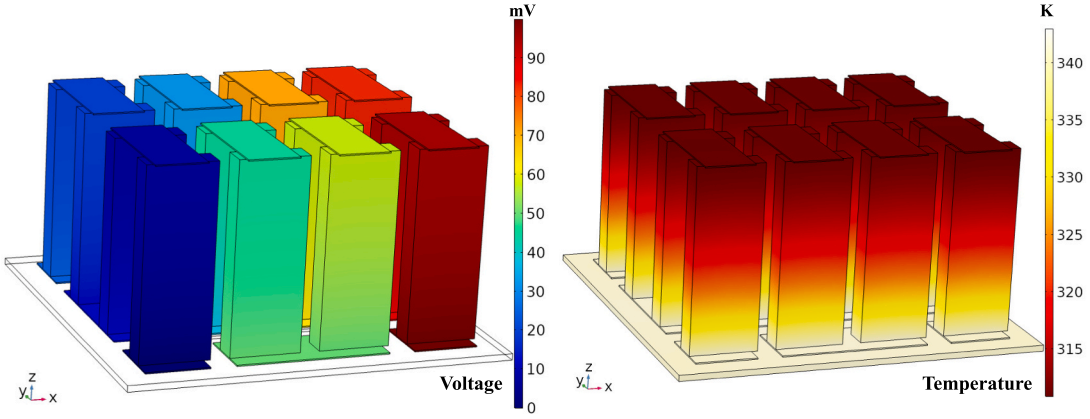

(b)

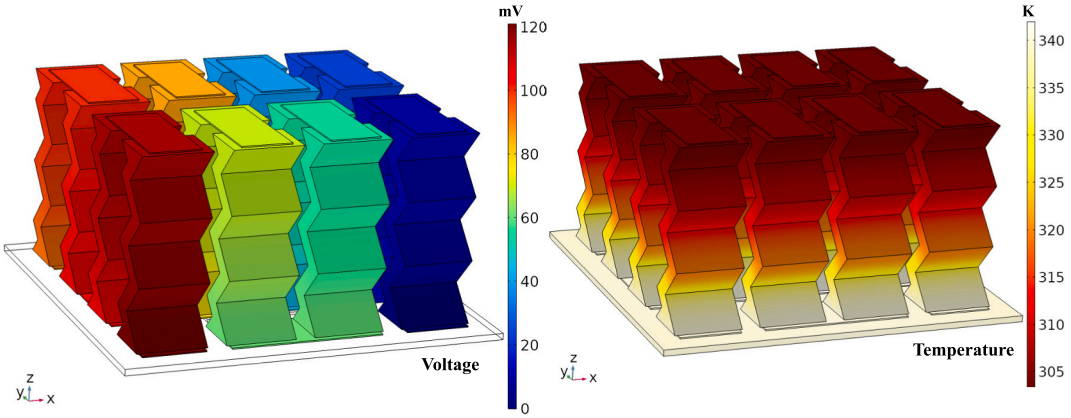

(c)

Fig. 7. Numerical distribution diagram obtained from the simulation of different heat recovery modes in COMSOL. (a) Temperature thermal zone diagram of TPV cell at 1000 K heat source temperature. Potential and temperature distributions of (b) I-type, (c) W-type TE-HRL and (d) TE wi-HSF at 1000 K heat source temperature. (e) Trend of TPV cell temperature and TE temperature difference with different heat source temperature.

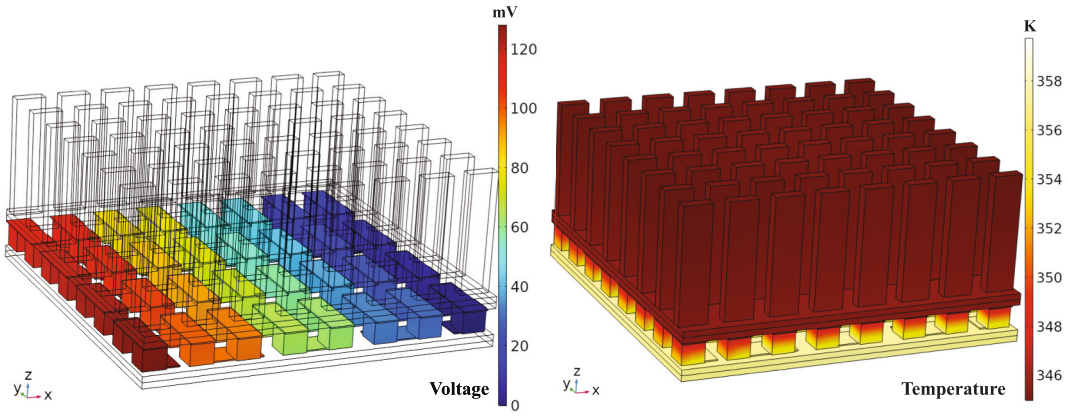

(d)

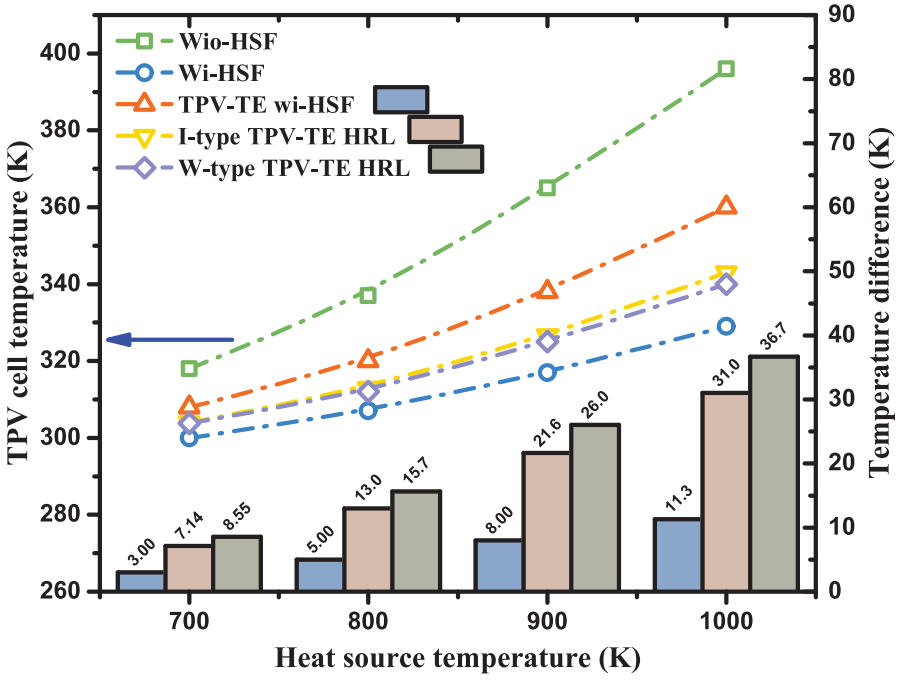

(e)

Fig. 7. (*continued*).

model is the ratio of the output of TPV and TE to the incident radiant energy. Parameters specifically related to the simulations and calculations described in this section have been listed in Table S1–3 of the Supplementary Information.

2.3. Characterizations of thermoelectric materials for TE-HRL

The thermoelectric material properties of the TE-HRL prepared by the cold–press moulding and sintering method were further analyzed. The thermoelectric parameters at different temperatures were measured using thermoelectric parameter measurement system (Cryoall CTA) and thermal conductivity tester (DRL-III), while the power factor ($PF = \alpha^2\sigma$) and TE figure of merit ZT ($ZT = PF{\cdot}T/\kappa$) were calculated from the Seebeck coefficient, the electrical and thermal conductivity.

2.4. Experimental method for RTPV-TE heat recovery

Fig. 5 shows the electrical output test system of the InGaAs cells with the TE-HRL. The programmable linear DC power supply (DP832A, RIGOL Technologies Inc.) power provides power to the central heat source bar, which has a surface temperature range of 700–1000 K. The temperature of the InGaAs TPV cell and TE-HRL was determined using a temperature-measuring instrument (R7100). The electrical performance of the InGaAs cell and TE-HRL was tested with a parameter analyzer (Keithley 4200 SCS) in a dark environment with a normal temperature of 293.15 K and standard atmospheric pressure of 1 atm. In error analysis [42], electrical and temperature tests for each heat source temperature point were carried out after the experimental system had been stabilized for 30 min and had reached thermal equilibrium in order to minimize measurement errors. Then, for each key data, a set of sequence was obtained after recording 5 times. The mean and standard deviation of this set of values were calculated and then plotted as the Figures in this paper. Specific data error calculations have been listed in Tables S5 and S6 of the Supplementary Information. In addition, another error-producing factor is the inherent error carried by the measuring instruments itself in the experiment. The temperature-measuring

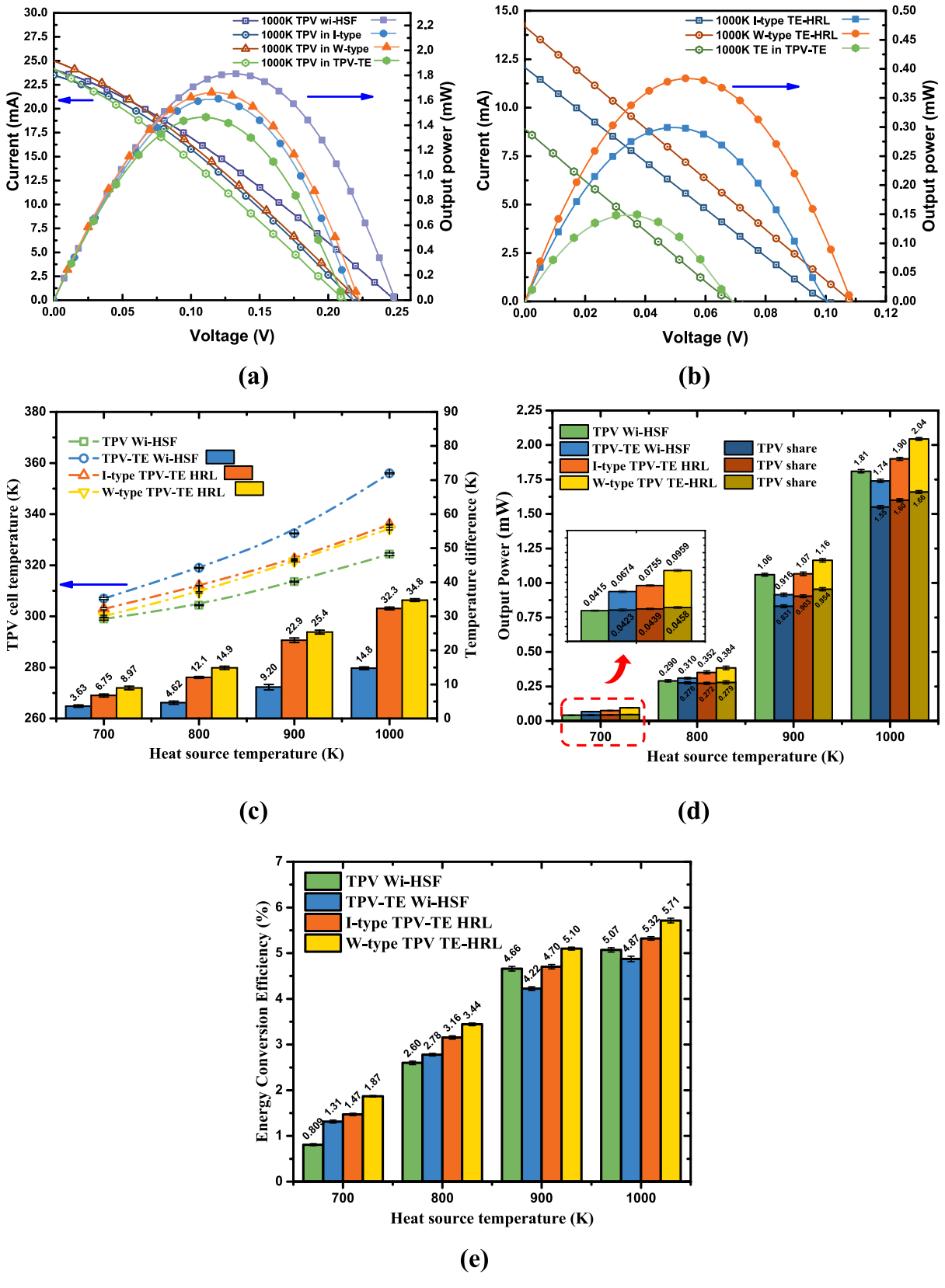

Fig. 8. The *I–V*/*P–V* curves of (a)TPV cells and (b) TE RHLs were measured at 1000 K heat source temperature. The (c) temperature of TPV cell, (d) output power and (e) efficiency with heat source temperature for each heat recovery module.

instrument (R7100) has an inherent error of ±0.1%, from which the error in the calculated temperature difference is ±0.2%. And the parameter analyzer (Keithley 4200 SCS) has an inherent error of ±0.04% for current and voltage tests, and an error of ±0.08% for the calculated output power. The value of the measurement deviation due to the inherent error of the measuring instruments is very minimal, so this has a very limited effect on the data obtained from the experiment.

3. Result and discussion

3.1. Material characterization analysis of TE-HRL

The thermoelectric properties of TE-HRL prepared using the cold-press moulding and sintering method were evaluated by experimental test characterization, as shown in Fig. 6. The prepared P/N-type TE-HRL showed good Seebeck coefficients in the low-temperature range of 300–400 K, which varied in the range of 235–271 μV/K for P-type and −177 – −170 μV/K for N-type, shown in Fig. 6(a). In terms of conductivity, compared with the P-type material, the N-type material shows better conductivity at the corresponding temperatures, thus reaching 3.10×10^4–3.95×10^4 S/m, shown in Fig. 6(b). Fig. 6(c) shows that the PF decreases with increasing temperature, and the N-type also has a better conductivity than the P-type, reaching 1132 μW/K^2·m at 300 K. In Fig. 6(d), the thermal conductivity of the P/N TE-HELs tested in the range of 300–400 K increases with increasing temperature and does not exceed 0.46 and 0.68 W/m·K, respectively. In Figs. 6(e) and (f), the ZT value of the P/N–type TE-HRL were obtained at 300 K, reaching 1.01 and 1.51, respectively. It is noteworthy that at 300–340 K, the ZT values of P-type TE-HRL prepared in this work is essentially flat compared to existing Bi_2Te_3-based inorganic thermoelectric paints, while the N-type is more competitive [39,43,44]. In this part, the excellent thermoelectric properties of the prepared TE-HRL were characterized and analyzed, laying the foundation for its subsequent heat recovery for TPV-TE module.

3.2. Simulation and comparative analysis

The temperature and potential simulation results for various types of TPV heat recovery models in COMSOL were presented in Fig. 7. Firstly, the hot zone distribution of the TPV cell surface temperature for different heat recovery models were plotted in Fig. 7 (a). Temperature distribution curves of TPV cell in different heat recovery modes at 1000 K heat source temperature also shown in Fig. S1, the temperature distribution with position is Gaussian over the entire TPV cell surface. TPV cell without HSF has the highest temperature (397 K) and its thermal zone varies also considerably between the center and the periphery, which greatly affects efficiency and uniformity of carrier collection in the TPV cell and limits its photovoltaic performance. Previous studies have shown that for every 10 K increase in TPV cell temperature from 300 K, the output power decreases by 13.7%, and at a temperature of 373 K, the output of the TPV cell is close to zero [14]. Therefore, the TPV cell without HSF will have no electrical output due to the high temperature. The TPV-TE wi HSF also has a high temperature of 360 K, so the output power of its TPV cell is also severely degraded. From the temperature distribution in Fig. 7 (d), it can be concluded that most of the heat is accumulated at the TPV cell and is difficult to be conducted out by the HSF, which seriously affects its output performance. Hence the design of TPV-TE wi HSF is not reasonable for the TPV system.

However, the difference of I/W TE-HRL in surface temperature of the TPV cells can be maintained within 2 K, and has a much lower temperature (<340 K). At the same time, the surface of TPV cell has a smaller and more homogeneous thermal zone, which contributes to the efficiency of the photovoltaic conversion. From Figs. 7(b) and (c), it can also be seen that the temperature distribution of the I and W TE-HRL module are uniform, and the heat that reaches the TPV cell can be smoothly conducted out, which is more reasonable than the mainstream TPV-TE wi HSF solution.

Fig. 7(e) demonstrates the trend of temperature and temperature difference of each mode with the temperature of the heat source, which are both rising with the heat source temperature. The TPV wio HSF and TPV-TE wi HSF due to poor heat dissipation, both TPV cell temperatures rise rapidly. The I/W-type TPV-TE HRL has a smoother rise in TPV cell temperature due to the reasonable structure design, while the W-type is slightly lower than the I-type. Compared to I-type, the W-type TE-HRL has a larger heat dissipation area (single-leg surface area raised from 247 to 349 mm^2) and a more tortuous heat transfer path (increased from 15 to 21 mm), thus allowing for greater temperature and potential differences. However, the TE with HSF was much inferior in terms of temperature and potential difference due to heat transfer and size limitations. The TPV cell with HSF exhibits the most effective heat dissipation and the lowest temperature, making it a standard reference for evaluating the heat recovery performance of the three aforementioned modes. The HSF-equipped design is a conventional and representative approach in the current device design, which is widely used and typical.

In this section, based on the simulation results of COMSOL, the advantages and disadvantages of each mode for the heat dissipation and heat recovery characteristics were preliminarily evaluated. The simulation data provides a good reference sample, which helps to analyze the results of the following experimental tests.

3.3. Analysis of experimental test results

Experimental test results for TPV cell and TE in different heat recovery modes were shown in Fig. 8, and more *I-V/P-V* curves at heat source temperature were shown in Supporting Information (Figs. S3–6). The *I-V/P-V* curves for different modes of TPV cells and TE at 1000 K heat source temperature were selected and shown in Fig. 8 (a-b). For TPV cell, the main difference between the *I-V/P-V* curves of different models was reflected in V_{oc} and P_{max}. For the TE, there are significant differences in the *I-V/P-V* curves for different modes. The variation of the above parameters can be derived from the temperature and temperature difference data obtained from the experimental tests, as shown in Fig. 8 (c). Its comparison with the simulation results in Fig. 7 (e) shows that the temperature and temperature difference of each mode obtained from the experimental test basically match the trend of the simulation, and the integrated error of the TPV cell temperature is 1.013%, and the integrated error of the TE temperature difference is 5.163%. The experimental test and the simulation data confirm each other. And for the results of the experimental tests, the errors, which are mainly in the systematic errors resulting from the numerical measurement process, have been added to the data of each experimental test and were reflected in the data plots in the form of error bars. These errors are small enough and do not significantly affect the conclusions drawn from the analysis of the data.

The lower the temperature of a TPV cell, the higher the V_{oc} and P_{max} in its output *I-V/P-V* curves, while the influence of temperature on I_{sc} was less pronounced. Correspondingly, the temperature difference is the decisive factor for the TE section and is directly reflected in the I_{sc}, V_{oc}, and P_{max} of its *I-V/P-V* curves, the higher the temperature difference, the higher their values. It can also be concluded from the temperature trend graph that the I/W-type TE HRL design provides better heat dissipation and yields lower TPV cell temperatures than the mainstream solution of TPV-TE with HSF.

For further comparative analysis of the performance of the different heat recovery modes, the P_{max} of the *I-V/P-V* curve at each temperature was extracted for comparative analysis, as shown in Fig. 8 (d). For heat source temperatures ranging from 700 to 800 K, the mainstream TPV-TE with HSF solution shows certain power improvements compared to TPV with HSF. However, when the temperature increases to 900–1000 K, the output power starts to decrease. The main reason is that the mainstream heat recovery design cannot quickly dissipate heat, resulting in TPV cell temperatures reaching 330–356 K at this point, limiting its conversion of

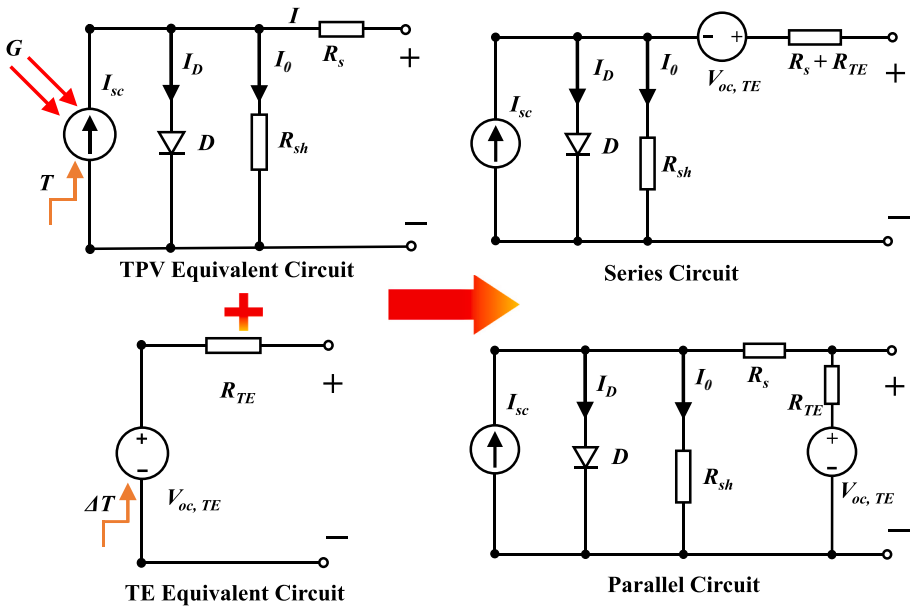

Fig. 9. Series-parallel equivalent circuit diagram of TPV and TE.

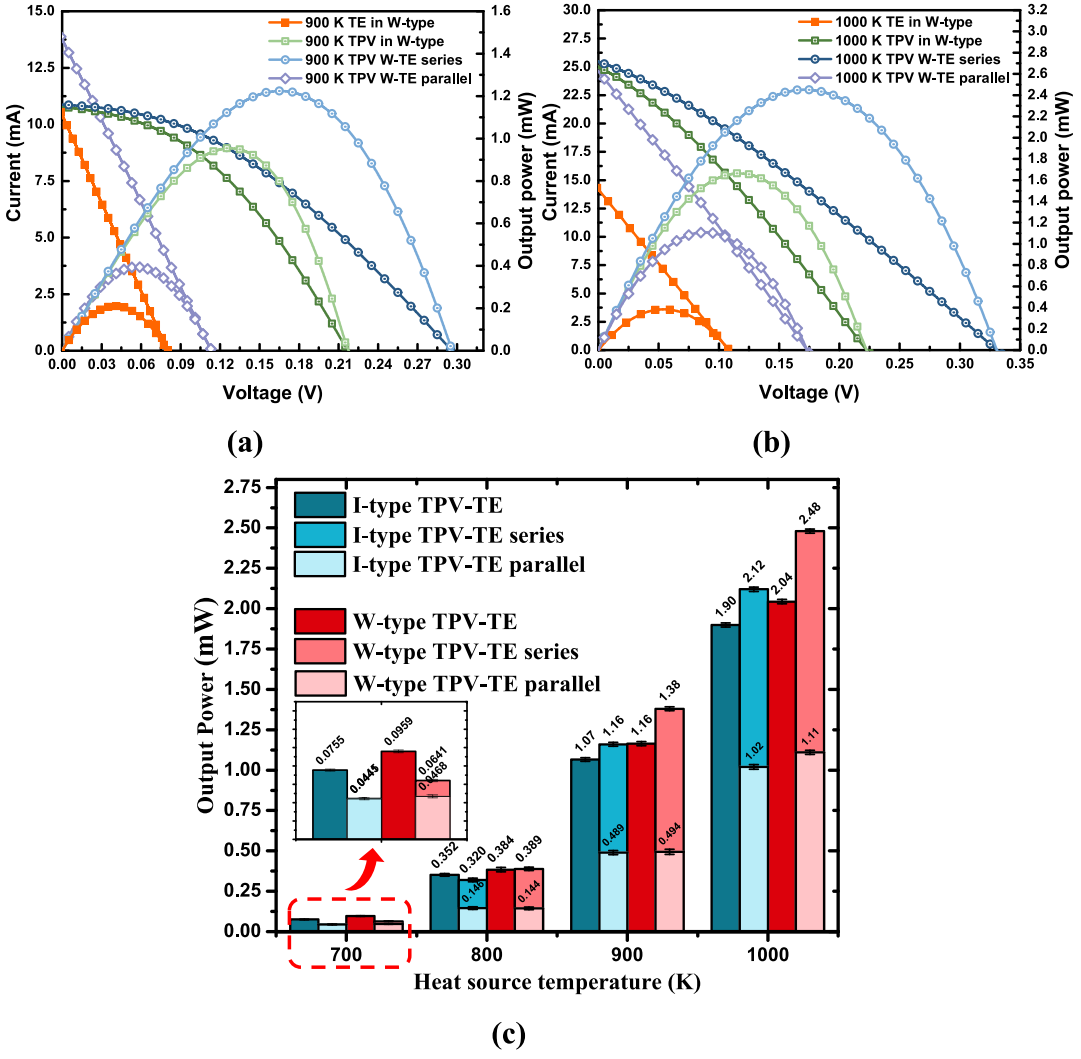

Fig. 10. At (a) 900 K and (b) 1000 K, the W-type TPV-TE HRL *I-V/P-V* curves for series-parallel circuit. (c) The P_{max} in the *P—V* curve was extracted as a trend with heat source temperature.

infrared radiation energy. Therefore, the performance enhancement of the mainstream TPV-TE with HSF solution is limited for RTPV systems operating at higher heat source temperatures.

In contrast, for the I/W-type TPV-TE heat recovery module, the output power at various temperatures was consistently higher compared to TPV with HSF. Additionally, the power enhancement of the W-type TE HRL is evidently superior to the I-type. Although the TPV cell equipped with the I/W-type TE-HRL experiences a decrease in the power fraction compared to the wi-HSF due to temperature effects, the heat recovery gain of the TE-HRL is greater, resulting in an overall positive power gain. At 1000 K heat source temperature, the W-type TPV-TE-HRL heat recovery mode shows a 17.24% increase in output power compared to the mainstream structure, while it achieves a 12.9% heat recovery gain compared to TPV with HSF.

The trends of energy conversion efficiency for each model with temperature variation were shown in Fig. 8 (e). As the heat source temperature increases, the energy conversion efficiency gradually improves for all heat recovery modes. However, the TPV with HSF shows a noticeable decrease in improvement magnitude at 900–1000 K. In contrast, the I/W-type TE RHL design proposed in this study achieves significant efficiency gains even at high heat source temperatures. At a heat source temperature of 1000 K, the W-type TPV-TE heat recovery module achieves an energy conversion efficiency of 5.71%.

3.4. Series-parallel study of TPV and TE

The TPV cell and TE HRL are two distinct yet interrelated energy conversion systems. In terms of electrical harvesting, it is possible to create separate circuits for energy harvesting based on the P_{max} of each system, but this would increase circuit complexity and results in higher energy losses. Instead, connecting the TPV cell to the TE HRL as a whole for energy harvesting can optimize the electrical harvesting circuit and reduce losses [45]. A single diode model simulates the electrical features of the TPV cell, and the TE device circuit is equated to a union of a voltage source and a series resistor, as shown in Fig. 9. Furthermore, the equivalent circuit diagrams of TPV before and after the series and parallel connection with TE have been presented, respectively. In the figure, G indicates the infrared radiation and the photogenerated current I_{sc} is affected by the temperature T. D is the corresponding value of the equivalent diode, and ΔT is the temperature difference between the hot and the cold ends of TE-HRL.

Figs. 10 (a) and (b) show the *I-V/P-V* curves for the TPV cell in series and parallel with the W-type TE HRL, and the series and parallel *I-V/P-V* curves for more modes were shown in Supporting Information (Figs. S7-S9). At 700–1000 K heat source temperature, the TPV-TE series connection patterns show a similar pattern of change. That is, regardless of the value between the I_{sc} of TE and TPV, the I_{sc} of the *I-V/P-V* curves in the series mode is consistent with that of TPV, while the V_{oc} is the sum of both TPV and TE. And P_{max} in series mode is always higher than TPV. However, the pattern of the parallel mode of TPV-TE at different heat source temperatures is difficult to be summarized, and P_{max} is always lower than TPV at 800–1000 K.

The main reason for this is that, the electrical output obtained was significantly lower due to the loop current generated in the circuit between TPV and TE in parallel mode, which leads to a significant internal consumption between the two electrical output modes and each other. While in series mode, the two barely interfere with each other, and the series design instead boosts the overall voltage, so the output power has a further increase.

Those P_{max} in the *P—V* curves were extracted and shown in Fig. 10 (c). At 800–1000 K, the output of the TPV cell in series with the TE HRL is always more than twice as high as in parallel, with the advantage of the series connection being more obvious. At 700–800 K, the P_{max} of the TPV-TE HRL series was lower than or equal to the sum of the two, while at 900–1000 K the series output was more advantageous than the sum of the two, further increasing the output power of the system. At 1000 K, TPV in series with W-type TE-HRL has 21.6% power increase compared to the sum of the two, the heat recovery gain is also increased to 37.0%. Thus, when the TPV-TE HRL heat recovery system was used for energy harvesting at high heat source temperatures, the combination of the two in a series circuit increases the output power of the system, and the W-type TE-HRL has a better power increase than the I-type.

Table 1
Comparison of the heat recovery gain between the existing PV-TE hybrid systems in the literature and this work.

Type	*Heat Recovery Gain (%)*	*Operation Conditions*	*PV*	*TE*	*Ref.*
Novel spectral splitting PV-TE hybrid system	**6.30** **6.80**	1 Sun concentration 1.5 Sun concentration	GaInP cell	Commercial TE module (Bi_2Te_3)	[35]
Hybrid CPV-TE module	**2.92**	37 Suns concentration	InGaP/InGaAs/Ge triple-junction cell	Commercial TE module (Bi_2Te_3)	[46]
PV-TE hybrid system with PCM	**4.41**	437 Suns concentration	InGaP/InGaAs/Ge triple-junction cell	Commercial TE module (Bi_2Te_3)	[47]
LCPV/T-TEG hybrid system	**1.87**	4 Suns concentration	Si cell	Commercial TE module (Bi_2Te_3)	[48]
CPV-TE hybrid generator	**~3**	50 Suns concentration	GaAs cell	Commercial TE module (Bi_2Te_3)	[15]
CPV-TE hybrid system	**20.2**	217 Suns concentration	GaAs cell	Commercial TE module (Bi_2Te_3)	[33]
W-type TPV-TE HRL Series	**37.0**	1000 K of heat source	InGaAs cell	Cold pressing mould and sintering (Bi_2Te_3)	This Work
I-type TPV-TE HRL Series	**17.1**				

The comparative analysis was carried out with other data obtained from experimental tests in the literature, and the TPV-TE-HRL in series mode designed in this study has a superior heat recovery gain, as shown in Table 1. Due to the differences in the structural dimensions and optical conditions of the models, this serves only as a simple reference for comparison.

3.5. Application environment optimization analysis

The most valuable potential scenarios for RTPV applications are Mars and deep space, so the best practical value of this solution cannot be fully realized by designing and testing only on Earth. Therefore, the I/W TPV-TE heat recovery system operational characteristics in the Mars and deep space environment were simulated and analyzed. The simulation parameters for the Mars and deep space environments have been presented in detail in Supporting Information. Firstly, to verify the reasonableness and acceptability of the simulation model, the electrical outputs obtained from the simulation calculations were compared with the experimental test results, as shown in Fig. 11(a). The results show that the output power derived from different models in the simulation is basically in agreement with the experimental test results, which proves that the simulation model is acceptable for the subsequent Mars and

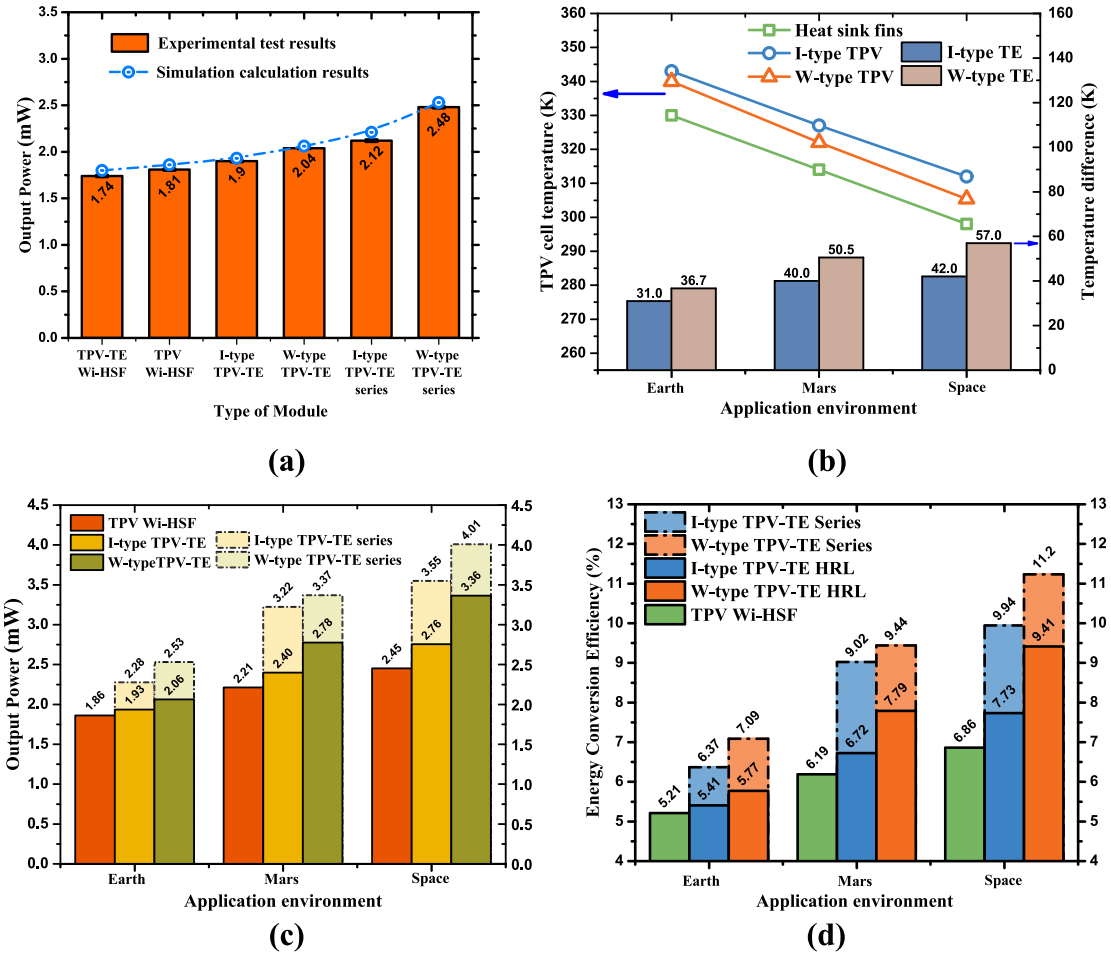

Fig. 11. (a) Comparison of Pmax obtained from simulation and experimental testing of each heat recovery model at 1000 K heat source temperature in the Earth environment. Trends in (b) temperature, (c) output power and (d) efficiency with application environment for each heat recovery model at 1000 K heat source temperature.

deep space performance simulation results.

The variation in temperature, temperature difference, output power and efficiency of the I/W TPV-TE heat recovery system at 1000 K heat source temperature has been shown in Figs. 11(b-d). As the application environment changes from Earth-Mars-deep space, the ambient temperature decreases significantly (from 300 K to 3 K), which causes the temperature of the TPV cell to decrease continuously, as shown in Fig. 11 (b). However, the high temperature heat source at 1000 K still provides a continuous high-density infrared radiation, so its temperature decrease is smaller than the ambient temperature (from 340 K to 310 K). However, this also significantly increases the difference in temperature between the TE-HRL and the ambient, which increases its radiative heat dissipation (Eq. 3) and facilitates the heat transfer of the system. In addition, the W-type TE-HRL has a larger surface area, so its corresponding TPV cell has a larger temperature drop, lower temperature, and larger temperature difference than the I-type. Because of the temperature drop of TPV cell and the enhancement of TE-HRL temperature difference, the output power and efficiency of the system are also significantly improved in both Mars and deep space environments, and the W-type heat recovery system has 63.10% output power improvement in deep space compared to on Earth. In addition, while the power gain from the series mode is equally significant in Mars and deep space environments, as shown in Fig. 11 (c).

Similarly, in Fig. 11 (d), the energy conversion efficiency varies with the application environment in a pattern consistent with the power, and the W-type heat recovery system achieves an energy conversion efficiency of 11.23% in the series mode. In contrast, the TPV wi-HSF without heat recovery is 6.86%, of which 4.37% of the energy is recovered, accounting for 39.0% of the total electrical output. The heat recovery power gain of the system in deep space is also improved, as shown in Table 2, where the heat recovery power gain of the W-type heat recovery system in series mode is increased from 36.0% on the Earth to 63.7% on deep space. The above results show that the TPV-TE heat recovery system designed in this work is more suitable for deep-space environment, and also prove that this solution can perform better power gain effect for RTPV under the condition of worse heat dissipation.

Table 2
Heat recovery gain for each module at different application environments.

Environment / *Heat recovery gain (%)*	*Earth*	*Mars*	*Space*
W-type TPV-TE HRL Series	36.0	52.5	63.7
I-type TPV- TE HRL Series	29.6	45.7	45.0
W-type TPV-TE HRL	10.8	25.8	37.2
I-type TPV-TE HRL	3.8	8.6	12.7

4. Conclusions

In this work, a novel I/W-type TPV-TE heat recovery system was proposed to achieve efficient energy utilization. The TE-HRL module was used as a heat sink to efficiently dissipate the heat from the TPV cell, while the residual heat of the RTPV system was further recovered and

converted into electrical energy using the thermoelectric effect. This solution improves the poor energy utilization of the RTPV system due to the large amount of wasted thermal energy, and further increases the output power and efficiency.

The I/W-type TE-HRL were prepared by cold press moulding and sintering and combined with InGaAs cells to form I/W TPV-TE heat recovery modules. The experimental and simulation results show that the proposed W-type TPV-TE heat recovery system can again improve the heat dissipation efficiency compared with previous commonly used schemes, and reduce the temperature of TPV cells from 360 K to 340 K at 1000 K heat source temperature. In addition, due to the convoluted structure and larger surface area of W-type TE-HRL, higher temperature difference and output power were obtained. Compared with the mainstream TPV-TE solution, the W-type TPV-TE heat recovery system improves the output power by 17.24% at 1000 K heat source temperature. And for TPV-HSF without employing heat recovery mode, the W-type TPV-TE has a heat recovery power gain of 12.9%, and with energy conversion efficiency of 5.71%. The TPV cells and TE-HRLs obtained higher output power in series mode at the heat source temperature of 1000 K, while the output power in parallel mode had a larger loss. The series mode of the W-type TPV-TE heat recovery system improved the output power by 21.6% over the independent mode. The series mode also allows further optimization of the circuit structure, which can be better matched with the subsequent energy harvesting system.

Simulation results for environmental applications show that the I/W TPV-TE heat recovery system was better suited to the deep space environment. The W-type TPV-TE-HRL has output gain of nearly 63.7% in series mode, with energy conversion efficiency of 11.23% at 1000 K heat source temperature. The insight from the laws of environmental study results is that the proposed scheme of using thermoelectric modules for heat dissipation and heat recovery in this paper is suitable for use in environments with poor heat dissipation. The proposed solution of using I/W-type TE-RHL as heat sink fins in this work can further improve the energy conversion efficiency and power of RTPV, enhance its competitiveness in space mission applications. And for this scheme, the direction of future refinement will be to optimize the size of TE-HRL according to the actual scenario, in anticipation of achieving a more excellent energy utilization.

CRediT authorship contribution statement

Hongyu Wang: Writing – review & editing, Writing – original draft, Supervision, Software, Methodology, Formal analysis, Data curation, Conceptualization. **Zhiheng Xu:** Writing – review & editing, Methodology, Funding acquisition, Formal analysis, Conceptualization. **Chen Wang:** Writing – review & editing. **Zongbin Hou:** Software. **Mingxin Bian:** Writing – review & editing, Conceptualization. **Nailiang Zhuang:** Writing – review & editing. **Haijun Tao:** Writing – review & editing. **Yuqiao Wang:** Writing – review & editing. **Xiaobin Tang:** Writing – review & editing, Methodology, Funding acquisition.

Declaration of Competing Interest

This paper has not been published or accepted for publication. It is not under consideration at another journals. No conflict of interest exists in the submission of this manuscript. All authors have read and approved this version of the article, and due care has been taken to ensure the integrity of the work.

Data availability

Data will be made available on request.

Acknowledgments

This work is supported by the National Natural Science Foundation of China (Grant Nos. 12275132 and 12075119), China Postdoctoral Science Foundation (Grant No. 2022 M711613), the Excellent Postdoctoral Program of Jiangsu Province (Grant No. 2022ZB235).

Appendix A. Supplementary data

Supplementary data to this article can be found online at https://doi.org/10.1016/j.apenergy.2023.122259.

References

[1] Yuan Z, Tang X, Xu Z, Li J, Chen W, Liu K, et al. Screen-printed radial structure micro radioisotope thermoelectric generator. Appl Energy 2018;225:746–54.
[2] Lange RG, Carroll WP. Review of recent advances of radioisotope power systems. Energ Conver Manage 2008;49:393–401.
[3] Zhang Z, Tang X, Liu Y, Xu Z, Ye H, Tian F, et al. Application of liquid scintillators as energy conversion materials in nuclear batteries. Sensors Actuators, A Phys 2019;290:162–71. https://doi.org/10.1016/j.sna.2019.03.024.
[4] Wang X, Liang R, Fisher P, Chan W, Xu J. Critical design features of thermal-based radioisotope generators: a review of the power solution for polar regions and space. Renew Sustain Energy Rev 2020;119:109572. https://doi.org/10.1016/j.rser.2019.109572.
[5] Cheon SJ, Hong SG, Lee JH, Nam YS. Design and performance analysis of a 500-W heat source for radioisotope thermophotovoltaic converters. Int J Energy Res 2018;42:817–29. https://doi.org/10.1002/er.3889.
[6] Lee J, Cheon S, Hong S, Nam Y. A radioisotope thermophotovoltaic converter with nanophotonic emitters and filters. Int J Heat Mass Transf 2017;108:1115–25. https://doi.org/10.1016/j.ijheatmasstransfer.2016.12.049.
[7] Wang X, Liang R, Fisher P, Chan W, Xu J. Radioisotope thermophotovoltaic generator design methods and performance estimates for space missions. J Propuls Power 2020;36:593–603. https://doi.org/10.2514/1.B37623.
[8] Ferrari C, Melino F, Pinelli M, Spina PR. Thermophotovoltaic energy conversion: analytical aspects, prototypes and experiences. Appl Energy 2014;113:1717–30.
[9] Datas A, Martí A. Thermophotovoltaic energy in space applications: review and future potential. Sol Energy Mater Sol Cells 2017;161:285–96. https://doi.org/10.1016/j.solmat.2016.12.007.
[10] Wang H, Tang X, Liu Y, Xu Z, Yuan Z, Liu K, et al. Thermal emission-enhanced and optically modulated radioisotope thermophotovoltaic generators. Energ Technol 2020:8. https://doi.org/10.1002/ente.201901170.
[11] Martín D, Algora C. Temperature-dependent GaSb material parameters for reliable thermophotovoltaic cell modelling. Semicond Sci Technol 2004;19:1040–52. https://doi.org/10.1088/0268-1242/19/8/015.
[12] Blandre E, Vaillon R, Drévillon J. New insights into the thermal behavior and management of thermophotovoltaic systems. Opt Express 2019;27:36340. https://doi.org/10.1364/oe.27.036340.
[13] Dupré O, Vaillon R, Green MA. Thermal Behavior of Photovoltaic Devices. 2017. https://doi.org/10.1007/978-3-319-49457-9.
[14] Wang H, Xu Z, Liu Y, Meng C, Tang X. Irradiation and temperature service stability of the radioisotope thermophotovoltaic generators based general purpose heat source. Prog Nucl Energy 2023;163:104807. https://doi.org/10.1016/j.pnucene.2023.104807.
[15] Kil TH, Kim S, Jeong DH, Geum DM, Lee S, Jung SJ, et al. A highly-efficient, concentrating-photovoltaic/thermoelectric hybrid generator. Nano Energy 2017;37:242–7. https://doi.org/10.1016/j.nanoen.2017.05.023.
[16] Wang X, Chan W, Stelmakh V, Celanovic I, Fisher P. Toward high performance radioisotope thermophotovoltaic systems using spectral control. Nucl Instruments Methods Phys Res Sect A Accel Spectrometers, Detect Assoc Equip 2016;838:28–32. https://doi.org/10.1016/j.nima.2016.09.028.
[17] Sakakibara R, Stelmakh V, Chan WR, Geil RD, Krämer S, Savas T, et al. A high-performance, metallodielectric 2D photonic crystal for thermophotovoltaics. Sol Energy Mater Sol Cells 2022;238:111536. https://doi.org/10.1016/j.solmat.2021.111536.
[18] Wang Y, Zhou L, Zhang Y, Yu J, Huang B, Wang Y, et al. Hybrid solar absorber–emitter by coherence-enhanced absorption for improved solar thermophotovoltaic conversion. Adv Opt Mater 2018;6:1800813.
[19] Li D, Xuan Y. Design and evaluation of a hybrid solar thermphotovoltaic-thermoelectric system. Sol Energy 2022;231:1025–36. https://doi.org/10.1016/j.solener.2021.12.049.
[20] Meng C, Liu Y, Xu Z, Wang H, Tang X. Selective emitter with core–shell nanosphere structure for thermophotovoltaic systems. Energy 2022;239:121884. https://doi.org/10.1016/j.energy.2021.121884.
[21] Wang H, Xu Z, Yuan Z, Liu K, Meng C, Tang X. High-temperature and radiation-resistant spinel-type ferrite coating for thermo-optical conversion in radioisotope thermophotovoltaic generators. Energy 2022;239:122255. https://doi.org/10.1016/j.energy.2021.122255.
[22] Wang J, Tang X, Zhao S, Deng H, Ji C, Wang H, et al. An efficient photon utilization radioisotope thermophotovoltaic based on curled reflectors. Energ Technol 2023;2201477:1–12. https://doi.org/10.1002/ente.202201477.
[23] Olabi AG, Al-Murisi M, Maghrabie HM, Yousef BA, Sayed ET, Alami AH, et al. Potential applications of thermoelectric generators (TEGs) in various waste heat recovery systems. Int J Thermofluids 2022;16:100249. https://doi.org/10.1016/j.ijft.2022.100249.

[24] Ochieng AO, Megahed TF, Ookawara S, Hassan H. Comprehensive review in waste heat recovery in different thermal energy-consuming processes using thermoelectric generators for electrical power generation. Process Saf Environ Prot 2022;162:134–54. https://doi.org/10.1016/j.psep.2022.03.070.
[25] Luo D, Sun Z, Wang R. Performance investigation of a thermoelectric generator system applied in automobile exhaust waste heat recovery. Energy 2022;238:121816. https://doi.org/10.1016/j.energy.2021.121816.
[26] Ge Y, Lin Y, He Q, Wang W, Chen J, Huang SM. Geometric optimization of segmented thermoelectric generators for waste heat recovery systems using genetic algorithm. Energy 2021:233. https://doi.org/10.1016/j.energy.2021.121220.
[27] Tang J, Ni H, Peng RL, Wang N, Zuo L. A review on energy conversion using hybrid photovoltaic and thermoelectric systems. J Power Sources 2023;562:232785. https://doi.org/10.1016/j.jpowsour.2023.232785.
[28] Sripadmanabhan Indira S, Vaithilingam CA, Chong KK, Saidur R, Faizal M, Abubakar S, et al. A review on various configurations of hybrid concentrator photovoltaic and thermoelectric generator system. Sol Energy 2020;201:122–48. https://doi.org/10.1016/j.solener.2020.02.090.
[29] Cotfas DT, Cotfas PA, Mahmoudinezhad S, Louzazni M. Critical factors and parameters for hybrid photovoltaic-thermoelectric systems; review. Appl Therm Eng 2022;215:118977. https://doi.org/10.1016/j.applthermaleng.2022.118977.
[30] Shittu S, Li G, Zhao X, Zhou J, Ma X, Akhlaghi YG. Experimental study and exergy analysis of photovoltaic-thermoelectric with flat plate micro-channel heat pipe. Energ Conver Manage 2020;207:112515. https://doi.org/10.1016/j.enconman.2020.112515.
[31] Shittu S, Li G, Zhao X, Ma X, Akhlaghi YG, Fan Y. Comprehensive study and optimization of concentrated photovoltaic-thermoelectric considering all contact resistances. Energ Conver Manage 2020;205:112422. https://doi.org/10.1016/j.enconman.2019.112422.
[32] Shittu S, Li G, Zhao X, Akhlaghi YG, Ma X, Yu M. Comparative study of a concentrated photovoltaic-thermoelectric system with and without flat plate heat pipe. Energ Conver Manage 2019;193:1–14. https://doi.org/10.1016/j.enconman.2019.04.055.
[33] Yin E, Li Q, Xuan Y. Experimental optimization of operating conditions for concentrating photovoltaic-thermoelectric hybrid system. J Power Sources 2019;422:25–32. https://doi.org/10.1016/j.jpowsour.2019.03.034.
[34] Lamba R, Kaushik SC. Modeling and performance analysis of a concentrated photovoltaic-thermoelectric hybrid power generation system. Energ Conver Manage 2016;115:288–98. https://doi.org/10.1016/j.enconman.2016.02.061.
[35] Alnajideen M, Min G. Hybrid photovoltaic-thermoelectric system using a novel spectral splitting solar concentrator. Energ Conver Manage 2022;251:114981. https://doi.org/10.1016/j.enconman.2021.114981.
[36] Kim YJ, Choi H, Kim CS, Lee G, Kim S, Park J, et al. High-performance monolithic photovoltaic-thermoelectric hybrid power generator using an exothermic reactive interlayer. ACS Appl Energy Mater 2019;2:2381–6. https://doi.org/10.1021/acsaem.9b00011.
[37] Zhang J, Xuan Y. An integrated design of the photovoltaic-thermoelectric hybrid system. Sol Energy 2019;177:293–8. https://doi.org/10.1016/j.solener.2018.11.012.
[38] Liu K, Tang X, Liu Y, Xu Z, Yuan Z, Zhang Z. Enhancing the performance of fully-scaled structure-adjustable 3D thermoelectric devices based on cold–press sintering and molding. Energy 2020;206:118096. https://doi.org/10.1016/j.energy.2020.118096.
[39] Liu K, Tang X, Liu Y, Xu Z, Yuan Z, Ji D, et al. Experimental optimization of small–scale structure–adjustable radioisotope thermoelectric generators. Appl Energy 2020;280:115907. https://doi.org/10.1016/j.apenergy.2020.115907.
[40] King A. Radiative processes in astrophysics. Phys Bull 1980;31:359. https://doi.org/10.1088/0031-9112/31/10/053.
[41] Shockley W. The theory of p-n junctions in semiconductors and p-n junction transistors. Bell Syst Tech J 1949;28:435–89.
[42] Holman JP. Experimental methods for engineers. 8th ed. 2021.
[43] Park SH, Jo S, Kwon B, Kim F, Ban HW, Lee JE, et al. High-performance shape-engineerable thermoelectric painting. Nat Commun 2016;7:1–10. https://doi.org/10.1038/ncomms13403.
[44] Choi H, Kim YJ, Kim CS, Yang HM, Oh MW, Cho BJ. Enhancement of reproducibility and reliability in a high-performance flexible thermoelectric generator using screen-printed materials. Nano Energy 2018;46:39–44. https://doi.org/10.1016/j.nanoen.2018.01.031.
[45] Yin E, Li Q. Achieving extensive lossless coupling of photovoltaic and thermoelectric devices through parallel connection. Renew Energy 2022;193:565–75. https://doi.org/10.1016/j.renene.2022.05.054.
[46] Mahmoudinezhad S, Rezania A, Cotfas DT, Cotfas PA, Rosendahl LA. Experimental and numerical investigation of hybrid concentrated photovoltaic – thermoelectric module under low solar concentration. Energy 2018;159:1123–31. https://doi.org/10.1016/j.energy.2018.06.181.
[47] Li D, Xuan Y, Yin E, Li Q. Conversion efficiency gain for concentrated triple-junction solar cell system through thermal management. Renew Energy 2018;126:960–8. https://doi.org/10.1016/j.renene.2018.04.027.
[48] Haiping C, Jiguang H, Heng Z, Kai L, Haowen L, Shuangyin L. Experimental investigation of a novel low concentrating photovoltaic/thermal–thermoelectric generator hybrid system. Energy 2019;166:83–95. https://doi.org/10.1016/j.energy.2018.10.046.